



The Four-Sinker Densimeter: A New Instrument for the Combined Investigation of Accurate Densities and Sorption Phenomena of Pure Gases and Gas Mixtures

Luca Bernardini¹ · Reiner Kleinrahm² · Katharina Moritz¹ · Mark O. McLinden³ · Markus Richter¹

Received: 3 December 2023 / Accepted: 23 January 2024 / Published online: 29 February 2024
© The Author(s) 2024

Abstract

An apparatus for high-accuracy gas density and adsorption measurements over the range of temperature from (193 to 423) K and pressure from (0 to 15) MPa is described. This instrument is based on the two-sinker densimetry principle and incorporates a magnetic suspension balance. In addition to the two “density sinkers”, two “sorption sinkers” are weighed to investigate density and adsorption of a gas sample simultaneously. The design of the sinkers increases the resolution of density and adsorption investigations and enables the correction of sorption effects on density measurements. The complete apparatus, including the sinkers, the temperature and pressure measuring systems, and the measurement procedure, is described. For the density range investigated, the uncertainty ($k = 2$) is between (0.0034 to 0.019) $\text{kg}\cdot\text{m}^{-3}$, corresponding to (0.060 to 0.011)%. The uncertainty ($k = 2$) in adsorption load is (0.16 to 0.26) $\mu\text{g}\cdot\text{cm}^{-2}$. Density measurements at $T = (283 \text{ and } 293)$ K and pressures up to 10 MPa of high-purity argon and nitrogen validate the instrument for density. Adsorption measurements of high-purity carbon dioxide and propane on a gold surface validate the instrument for adsorption investigation at $T = (283 \text{ and } 293)$ K and up to the saturation pressure of the investigated gas. The apparatus was used to measure the binary mixture (0.75 $\text{CO}_2 + 0.25 \text{C}_3\text{H}_8$). In the future, the apparatus will also be used to accurately determine dew-point densities and pressures of pure gases and gas mixtures.

Keywords Binary gas mixture · Dew point · Dew-point density · Four-sinker densimeter · Gravimetric apparatus

Selected Papers of the 22nd European Conference on Thermophysical Properties.

Extended author information available on the last page of the article

1 Introduction

Accurate determination of pressure-density-temperature (p , ρ , T) properties is key for the development of precise thermodynamic models [1]. Up to now, the state of the art for measuring these properties relies on the utilization of densimeters based on a magnetic suspension balance [2, 3]. In these instruments, objects called sinkers are suspended in the investigated fluid and weighed in order to determine the fluid density. However, recent studies demonstrate that sorption on the sinkers' surfaces can distort density measurements, especially at conditions close to the dew line (errors as much as 0.10% already in the homogeneous gas phase) [4, 5]. These distorting effects arise from (1) increasing adsorption while approaching the saturation pressure for both pure gases and gas mixtures, and (2) selective adsorption of mixture components with a consequent shift of the composition in the homogeneous gas phase.

Even for the most accurate densimeters reported in literature, none are able to account for both types of distorting effects. For example, in a Single-sinker Densimeter (SSD) [6, 7] only one sinker is weighed, and the measuring technique does not allow for the determination and correction of the mass of the gas adsorbed on the sinker surface. In this case, correction of the measured density requires external knowledge of the mass adsorbed on the specific material and surface finish of the sinker used. In a Tandem-sinker Densimeter (TSD) [8, 9], a "sorption sinker" can be suspended together with a "density sinker" to simultaneously measure density and adsorption. However, since the material and surface finish of the two sinkers differs, it is not possible to correct for the effects of sorption on density measurements. Furthermore, the increased surface area of the sorption sinker ($A_S = 89.2 \text{ cm}^2$) is still not enough to enable for the detection of very small amounts of adsorbate. Additionally, the small volumes and volume difference of the two sinkers render low-density measurements difficult, and the resulting uncertainties are large. For these reasons, this measuring technique is limited in both density and adsorption resolution. To date, the most accurate measurements of density reported in literature are obtained using a Two-sinker Densimeter (2SD) [1, 2, 10, 11]. In this instrument, two sinkers with same mass but very different volumes are weighed independently to measure the density of a fluid. Both sinkers have the same surface area and finish, and, although it is not possible to quantify the sorption effects, it is possible to cancel the adsorbed mass from the computation of the density thanks to the differential method used to analyze the data. However, this requires that the surface characteristics of the two sinkers are nearly identical.

In this work, we present a new apparatus, namely the Four-sinker Densimeter (FSD) [12, 13], which utilizes two "density sinkers" and two "adsorption sinkers" to investigate density and adsorption of a gas simultaneously. The main objectives in the development of this new densimeter were: increasing of the resolution of density measurements thanks to the large volume difference between the "density sinkers"; increasing the resolution of adsorption investigation due to the large surfaces and surface difference of the "sorption sinkers" compared to the

density sinkers; achievement of a lower uncertainty for adsorption measurements; and simultaneous adsorption measurements and quantitative correction of density measurements via use of one sorption sinker with the same surface finish as the density sinkers. Moreover, the FSD will be employed to measure adsorption on both pure gases and gas mixtures. This approach aims to validate molecular dynamics simulations, thus, enhancing our understanding of the adsorbate composition on an atomistic scale. It will also enable the correction of mixture density measurements, accounting for the composition shift resulting from selective adsorption of various components.

2 Apparatus Description

The Four-sinker Densimeter is based on the two-sinker densimetry technique and utilizes a magnetic-suspension balance [14]. The instrument was designed for the combined measurement of accurate densities and investigation of sorption phenomena over the temperature range (193 to 423) K and for pressures up to 15 MPa. The weighings of two "density sinkers" are used to calculate the density of the investigated gas, while two "sorption sinkers" are weighed to determine and correct adsorption phenomena, especially those that arise close to the dew line. Additionally, weighings of two compensation masses (a tantalum calibration mass and a copper tare mass) are used to determine the tare and calibration parameters of the analytical balance. A photograph of the entire apparatus is shown in Fig. 1. The massive aluminum frame supports all the key components, while the electrical instruments and the gas dosing system are located in the metal rack on the left.

2.1 Operation Principle

By weighing the six objects mentioned above (four sinkers and two compensation masses) it is possible to obtain a system of equations that allows for the determination of density and adsorption. Each equation writes out the forces contributing to the balance reading, consisting of the calibrated mass placed on, or suspended from, the balance pan together with the buoyancy forces acting on the mass. Furthermore, for the sinkers, the mass of adsorbed gas and its buoyancy correction are also considered.

Using the weighings of the tantalum calibration mass, W_{cal} , and the copper tare mass, W_{tare} , it is possible to obtain α , the balance calibration factor, and β , the tare parameter, according to the system of Eqs. 1 and 2. The factor α accounts for the fact that the calibration of the balance is performed in air using reference masses, while the sinkers are weighed while immersed in the investigated gas. The parameter β includes all the masses that are permanently suspended at the weighing line (e.g., the permanent- and electro- magnet, and the lifting rod), considering also their buoyancy force and adsorption of a gas on their surface [12], and for the empty balance pan reading (with no sinker or compensation mass weighed), which might differ from 0.



Fig. 1 Photograph of the apparatus. The key components from left to right are: vacuum pumps rack; gas cylinder; instruments and gas dosing system rack; core of the apparatus with the linear motors cage and the analytical balance at the top, and the insulation cylinder containing the measuring cell at the bottom; thermostat bath

$$W_{\text{cal}} = \alpha \cdot [(m_{\text{cal}} - \rho_{\text{air}} \cdot V_{\text{cal}}) + \beta] \quad (1)$$

$$W_{\text{tare}} = \alpha \cdot [(m_{\text{tare}} - \rho_{\text{air}} \cdot V_{\text{tare}}) + \beta] \quad (2)$$

where m and V are the calibrated mass and volume of the tantalum calibration mass (subscript "cal") and the copper tare mass (subscript "tare"). The density of the air for the balance environment, ρ_{air} , was calculated with the empirical Eq. 3, developed in our working group, based on the environmental conditions (T_{air} , p_{air} , and φ_{air}) measured via a data logger (OPUS 20 THIP, Luftt, Germany)¹:

$$\rho_{\text{air}} = \rho_{\text{air},0} \cdot \frac{p_{\text{air}}}{p_0} \cdot \frac{T_0}{T_{\text{air}}} \cdot \left(1 - 0.378 \cdot \frac{\varphi_{\text{air}} \cdot p_s(T_{\text{air}})}{p_{\text{air}}} \right), \quad (3)$$

¹ Commercial equipment, instruments, or materials are identified only in order to adequately specify certain procedures. In no case does such identification imply recommendation or endorsement by the National Institute of Standards and Technology, nor does it imply that the products identified are necessarily the best available for the purpose.

where $\rho_{\text{air},0} = 1.188 \text{ kg} \cdot \text{m}^{-3}$ is the density of dry air at $T_0 = 293.15 \text{ K}$ and $p_0 = 0.1 \text{ MPa}$, and φ_{air} is the relative humidity of the air. $p_s(T_{\text{air}})$ is the vapor pressure of water at the temperature T_{air} and is calculated using Eq. 4:

$$p_s(T_{\text{air}}) = 0.00206 \text{ MPa} \cdot e^{18.285 \cdot \left(1 - \frac{291.15 \text{ K}}{T_{\text{air}}}\right)} \tag{4}$$

Using the weight of the four sinkers, W_i (with subscript $i = 1$ to 4 depending on the sinker), and the previously determined α and β , it is possible to obtain a system of four equations. Sorption phenomena can be investigated by assuming that the amount of adsorbed material is proportional to the surface area and dependent on the surface finish of the sinkers. In this way, the mass adsorbed on each sinker, $m_{\text{sorp},i}$, can be expressed according to Eq. 5,

$$m_{\text{sorp},i} = \gamma_i \cdot A_{S,i} \tag{5}$$

in which γ_i is a proportionality factor expressing the adsorption load on the two surface finishes between the four sinkers: polished and gold plated for sinkers 1, 2 and 3; rough stainless steel for sinker 4 ($\gamma_1 = \gamma_2 = \gamma_3 \neq \gamma_4$). $A_{S,i}$ indicates the surface area of each sinker. This is calculated from the geometrical area, extrapolated from the CAD drawings, multiplied by a surface enlargement factor (SEF). To account for the roughness on smaller scale of the surface areas, which extends the surface available for adsorption, a SEF was determined for each sinker. The determination of this factor will be described in detail in future works. The elaborated procedure uses x-y-z datapoints from Raman microscopy to approximate the surface enlargement using a mesh.

Based on these assumptions, the system can be expressed by Eqs. 6–9, which together allow for the calculation of four outputs: ρ_{fluid} , the density of the investigated fluid; γ_3 and γ_4 , the two adsorption loads; and ϕ , the coupling factor that accounts and corrects the force transmission error [8, 15]. Specifically,

$$W_1 = \alpha \cdot \left[\phi \cdot \left\{ (m_1 + \gamma_3 \cdot A_{S,1}) - \rho_{\text{fluid}} \left(V_1 + \frac{\gamma_3 \cdot A_{S,1}}{\rho_{\text{cond}}} \right) \right\} + \beta \right] \tag{6}$$

$$W_2 = \alpha \cdot \left[\phi \cdot \left\{ (m_2 + \gamma_3 \cdot A_{S,2}) - \rho_{\text{fluid}} \left(V_2 + \frac{\gamma_3 \cdot A_{S,2}}{\rho_{\text{cond}}} \right) \right\} + \beta \right] \tag{7}$$

$$W_3 = \alpha \cdot \left[\phi \cdot \left\{ (m_3 + \gamma_3 \cdot A_{S,3}) - \rho_{\text{fluid}} \left(V_3 + \frac{\gamma_3 \cdot A_{S,3}}{\rho_{\text{cond}}} \right) \right\} + \beta \right] \tag{8}$$

$$W_4 = \alpha \cdot \left[\phi \cdot \left\{ (m_4 + \gamma_4 \cdot A_{S,4}) - \rho_{\text{fluid}} \left(V_4 + \frac{\gamma_4 \cdot A_{S,4}}{\rho_{\text{cond}}} \right) \right\} + \beta \right] \tag{9}$$

where m is the calibrated mass for each sinker. V is obtained using the calibrated volume V_0 at standard conditions ($T_0 = 273.15 \text{ K}$, $p_0 = 101 \text{ kPa}$) and correcting it for changes in the experimental T and p according to Eq. 10:

$$V = V_0 \cdot [1 + 3 \cdot \alpha_L \cdot (T - T_0) - (p - p_0)/K], \quad (10)$$

where α_L is the average linear thermal expansion coefficient (in the temperature range from T_0 to T), and K is the bulk modulus for the sinker material.

In the system described by Eqs. 6–9, ρ_{cond} is the assumed density of the condensate and is dependent on the investigated gas. Many different assumptions are available in literature. For example, for fluids at supercritical state it is assumed that ρ_{cond} equals the saturated liquid density at the standard boiling pressure of 0.1 MPa [9, 16]. In this work, ρ_{cond} for argon and nitrogen was calculated using the software REFPROP [17] and is respectively (1.3962 and 0.80659) $\text{g} \cdot \text{cm}^{-3}$. For fluids at subcritical conditions, for which molecular dynamics simulation were conducted to calculate the density of the condensate [18] (carbon dioxide and propane), ρ_{cond} can be expressed as a function of the ratio of the bulk density and the dew-point density. This assumption provides a more accurate value depending on the vicinity to the dew line and is simultaneously independent of the investigated temperature. For all other pure gases and gas mixtures in subcritical conditions, ρ_{cond} is calculated as the saturated liquid density at the investigated temperature T [8, 16].

For validation, calibration, and comparison purposes the experimental density, ρ_{exp} , is compared to the density calculated using a reference equation of state (EOS), ρ_{EOS} , via calculation of the relative deviation, as shown in Eq. 11:

$$\frac{\text{Rel.Dev.}}{\%} = 100 \cdot \frac{\rho_{\text{exp}} - \rho_{\text{EOS}}}{\rho_{\text{EOS}}}. \quad (11)$$

ρ_{EOS} is determined using the experimental T and p , and, in case of mixtures, the composition of the gas specified by the supplier.

2.2 Apparatus Design

A schematic of the FSD is presented in Fig. 2. Weight measurements are conducted with microgram resolution up to 62 grams using a customized analytical balance (Cubis MSA66S-000-DH, Sartorius, Germany). This balance is placed on top of the frame under a Plexiglas hood and incorporates two compensation masses, respectively made of copper and tantalum, along with a changing device.

An enlarged schematic of the magnetic suspension coupling (MSC) and the measuring cell containing the four sinkers is shown in Fig. 3. The MSC consists of an electro-magnet (at environmental conditions) suspended from the analytical balance with a long stem that runs inside a stainless steel tube. A permanent-magnet connected to the top of a lifting rod is magnetically coupled to the electro-magnet and is suspended inside the measuring cell where it is subject to experimental conditions. This magnetic coupling allows for the contactless transmission of the sinkers' weight to the analytical balance. The magnetic coupling is located inside the coupling housing, which separates the measuring environment from the balance environment. The housing is a hollow cylinder with a 2 mm thick separation wall and is made entirely of Copper-Beryllium (CuBe_2), a nonmagnetic material necessary

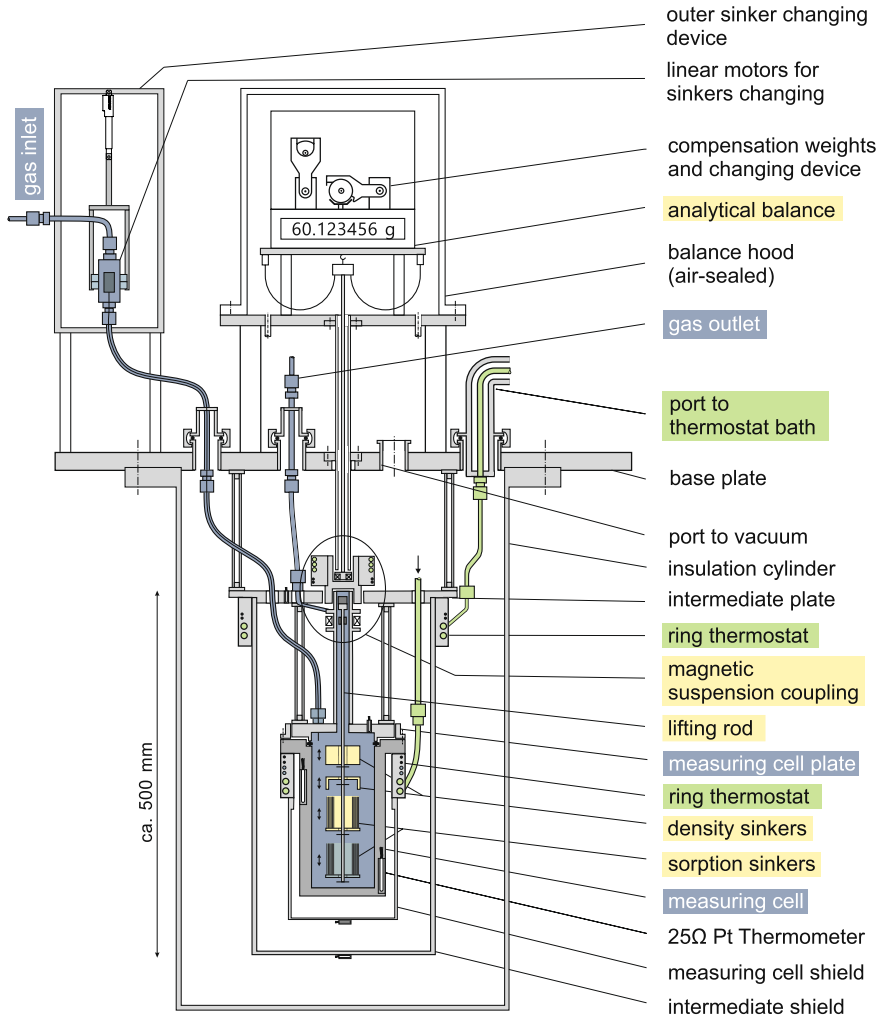
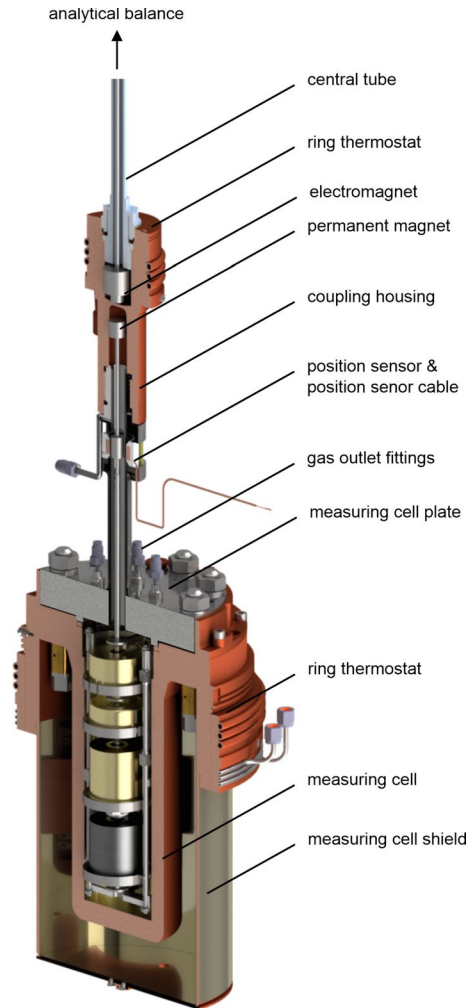


Fig. 2 Schematic of the four-sinker densimeter [12]. The main components from top to bottom are: outer sinker changing device (linear motors cage); analytical balance; magnetic-suspension coupling; measuring cell containing the four sinkers and the main thermometers; and temperature controlled shield and insulating shield

to avoid any impact on the magnetic coupling and to achieve stable measuring conditions.

The measuring cell is made of a high copper alloy (CuCr1Zr) and has an internal volume of about 632 cm³. It is gold plated inside, to resemble the surface finish of the gold-plated sinkers, and nickel-plated outside for surface hardening and to serve as a radiation shield. The cell contains the four sinkers, described below, and the inner changing mechanism, which is made entirely of stainless steel.

Fig. 3 Enlarged schematic of the magnetic suspension coupling (MSC) and the measuring cell containing the four sinkers. The main components of the MSC are: an electro magnet; a permanent magnet; the coupling housing; and a positions sensor. Inside the measuring cell two "density sinkers" are at the top and two "sorption sinkers" are at the bottom



The measuring cell is sealed together with the measuring cell plate using a copper ring. The plate, made of Inconel 625, hosts the inlet and outlet connections for the gas dosing. Stainless steel tubing run, from these connections, through the intermediate and base plate, up to the linear motors cage, and to the gas dosing system.

2.2.1 Sinkers

The four sinkers and the inner sinker changing mechanism are housed inside the measuring cell. The sinkers are shown in Fig. 4; each design offers a unique advantage to the measurement technique.

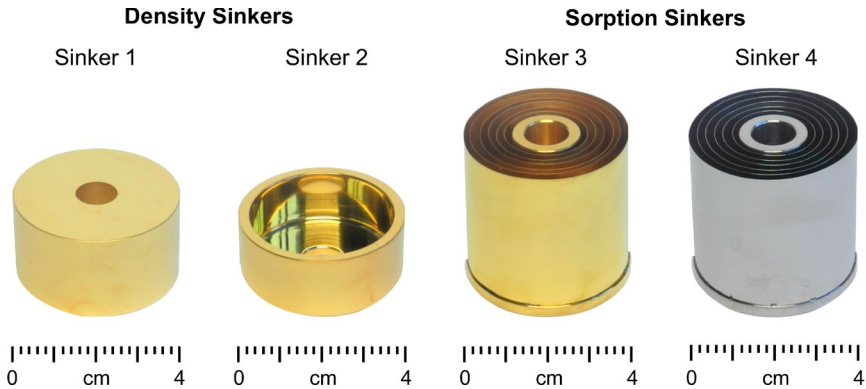


Fig. 4 Photograph of the four sinks. From left to right: density sinker 1 made of silicon with polished gold-plated surface; density sinker 2 made of stainless steel with polished gold-plated surface; sorption sinker 3 made of stainless steel with polished gold-plated surface; sorption sinker 4 made of stainless steel with rough surface. Sinks 3 and 4 are each comprised of six stainless steel rings welded to a bottom plate for an increased surface area

The two density sinks are at the top of the measuring cell; sinker one (S1) is made of single-crystal silicon and sinker two (S2) is made of stainless steel. Both are polished and gold plated in order to minimize sorption effects. They have almost the same mass and the same surface ($m \approx 60$ g, $A \approx 57$ cm²). S1 has a much larger volume ($V_{S1} \approx 25.7$ cm³ $\approx 3.38 \cdot V_{S2}$) in order to increase the buoyancy force acting on it and thus enhance the resolution for density measurements.

The two sinks at the bottom are the sorption sinks. Both are made of stainless steel and have the same geometry ($m \approx 60$ g, $V \approx 7.6$ cm³, $A \approx 440$ cm²), but their surface finishes are different. Sinker three (S3) is polished and gold plated so it has a similar surface finish to the density sinks; it is used to estimate and correct for the sorption effects on density measurements. Sinker four (S4) has a rough surface and is used to estimate the sorption phenomena on stainless steel. The large surface of the sorption sinks compared to the density sinks (ratio of 7.7) is achieved by six rings that are welded to a bottom plate, and results in improved resolution for adsorption measurements.

The masses of the sinks, as well as those of the compensation masses, were calibrated using an analytical balance (Cubis MCM-106, Sartorius, Germany) by means of the double substitution method [19]. The estimated combined standard uncertainty in the calibrated masses, $u_c(m)$, ranges between (9 and 14) μ g. The volume of the sinks, as well as those of the compensation masses, were calibrated with a hydrostatic comparator available at the National Institute of Standards and Technology (NIST) that uses reference silicon standards [20]. The estimated combined standard uncertainty in the calibrated volumes, $u_c(V)$, ranges between (0.0001 and 0.0003) cm³. The calibrated masses and volumes for the sinks and compensation masses are reported in Table 1, along with the corresponding combined standard uncertainties. Also shown in the table are the resulting calculated densities.

Table 1 Calibrated mass (m), volume (V), and associated combined standard uncertainty ($u_c(m)$ and $u_c(V)$) for compensation masses and sinkers. Also shown are the calculated densities (ρ)

Object	Material	m / g	$u_c(m) / \text{g}$	V / cm^3	$u_c(V) / \text{cm}^3$	$\rho / \text{g} \cdot \text{cm}^{-3}$
Calib. mass	Tantalum	60.656237	0.000014	3.6370	0.0001	16.6775
Tare mass	Copper	32.834898	0.000009	3.6811	0.0001	8.9198
Sinker 1 (S1)*	Silicon	60.008413	0.000010	25.6872	0.0003	2.3361
Sinker 2 (S2)*	SS 1.4301	59.979830	0.000009	7.5716	0.0001	7.9217
Sinker 3 (S3)*	SS 1.4301	59.570500	0.000011	7.4564	0.0001	7.9892
Sinker 4 (S4)*	SS 1.4301	60.050183	0.000010	7.6102	0.0001	7.8907

* $A_{S1} \approx A_{S2} \approx 57 \text{ cm}^2$; $A_{S3} \approx A_{S4} \approx 440 \text{ cm}^2$

The position of the sinkers is controlled with linear motors used to suspend or remove the sinkers from the weighing line. Each sinker has its own positioning device, which is located outside the measuring cell, on top of the main frame. The movement of a linear motor controls the position of a strong annular magnet placed around a stainless steel tube, which is magnetically coupled with a soft iron core inside the tube that is in contact with the measured gas. At the soft iron core is connected a long wire that runs to the inside the measuring cell, which controls the position of the inner sinker changing mechanism and, hence, of the sinker.

The magnetic suspension coupling utilizes a controller from a commercial gravimetric sorption analyzer, which was modified for use with the heavier sinkers of the FSD. While this controller works well, future development of this apparatus will require the development of a controller specifically designed for the 60 g sinkers in the FSD.

2.2.2 Temperature System

Two temperature-controlled shields are connected to the measuring cell plate and to the intermediate plate. Both are made of copper and are nickel-plated. An aluminum insulation cylinder is connected at the base plate and surrounds the core of the apparatus. Utilizing a multi-stage roots vacuum pump (ACP15, Pfeiffer Vacuum, Germany), vacuum (10^{-1} hPa) is created inside this outer cylinder to insulate the apparatus from the external environment.

The temperature inside the measuring cell is controlled with the combined action of a thermostat bath and several heaters distributed across the apparatus. The thermostat bath (PROLINE Kryomate RP 3090 CW, LAUDA, Germany) utilizes ethanol as thermostat fluid to regulate the temperature between 193 K and 350 K, although the present tests are limited to temperatures above 273 K. The fluid is distributed via three lines, each one flows to a copper thermostat ring around the coupling housing, the intermediate shield, and the measuring cell shield. Several heating wires are located in strategical positions of the apparatus. The heating temperature is monitored using thermometers (PT-103, Lake Shore, US) and controlled using a controller (PTC10, Stanford Research System, USA). The design of the temperature control

system aims to reduce vertical gradients across the measuring cell, minimize oscillation and instability, and avoid gas condensation inside tubing.

The experimental temperature is measured using two 25.5 Ω Standard Platinum Resistance Thermometers (SPRT 162D, Rosemount Aerospace GmbH, Germany) installed inside a thermowell in close contact with the measuring cell. In order to measure any vertical temperature gradient, one thermometer is installed at the top of the measuring cell and the other at the bottom on the opposite side. The thermometers were previously calibrated, according to the ITS-90 [21], in the temperature range (234 to 505) K [13]. Within the scope of this work, the calibration was confirmed in-house at the triple point of water and the freezing point of indium for measurements in the range (273 to 430) K. A resistance bridge (1595A Super Thermometer, Fluke, USA) in conjunction with a 25 Ω reference resistor (5685A3, Tinsley, UK) is used to measure the resistance of the thermometers.

2.2.3 Filling and Pressure Measuring System

Gas cylinders can be connected to an automatic gas-dosing system, which regulates the pressure of the experimental gas inside the measuring cell. The experimental pressure is measured by three pressure transducers (DIGIQUARTZ Models: 2300A-101-CE / 31K-101-CE / 43K-101-CE, Paroscientific, Inc., US) that ensure high accuracy in three different pressure ranges: low – between 0 and 1 MPa (1 MPa included), medium – between 1 and 4 MPa, and high – from 4 to 15 MPa. The pressure transducers were calibrated in-house using a piston gauge (DH 5201, Desgranges & Huot, France). The readings of the pressure transducers are corrected by subtracting the pressure offset at vacuum. The final pressure, p , is obtained applying the hydrostatic head correction according to Eq. 12, to correct for the fact that the pressure transducers are at a different height than the measuring cell:

$$p = p_{\text{meas}} + \rho_{\text{EOS}} \cdot g \cdot h . \quad (12)$$

Here, ρ_{EOS} is the density of the experimental gas calculated with an accurate equation of state, g is the gravity acceleration calculated for the exact location of the instrument, and h is the difference in height between the pressure transducers and the measuring cell.

To allow the ventilation of the investigated gas and the discharge of the adsorbed molecules two vacuum pumps are used. To bring the measuring cell in low vacuum condition (10^{-2} hPa) a rotary vane pump (DUO 2.5 A, Balzers-Pfeiffer, Germany) is used. High vacuum (10^{-4} hPa) is reached by activating a turbo-molecular pump (HiCube 80 Eco, Pfeiffer Vacuum, Germany). The two pumps are installed in parallel, can be excluded by means of on-off valves, and are never used simultaneously.

2.3 Measurement Procedure

Measurements are conducted along isotherms and include vacuum and gas measurements. The first requirement is a constant temperature across the measuring cell which is achieved by first setting the thermostat bath setpoint to a lower temperature

than desired. The targeted temperature is then obtained by activating the electrical heaters or, for temperatures close to environment condition, using the small residual heat transfer from the environment to the measuring cell.

Vacuum measurements are necessary to calculate the pressure reading offset and the density offset, both to be used as corrections during the analysis of gas measurements. The pressure offset is the pressure transducer's reading of the evacuated measuring cell assuming optimal vacuum conditions, and it differs for each transducers. The density offset represents the "apparatus zero" [1] and is the calculated vacuum density that differs slightly from zero ($0.0016 \text{ kg} \cdot \text{m}^{-3}$ in average).

Gas measurements enable the determination of density, adsorption and all other outputs calculated with Eqs. 6–9. After a stable temperature is reached, the gas sample is dosed into the evacuated measuring cell. Depending on the type of investigation conducted, it is possible to fill the sample at the lowest or highest desired pressure. From this point, measurements are performed by automatically increasing or decreasing the pressure using the gas dosing system. After each pressure change a sufficient equilibration time is allowed before starting the actual measurement. This equilibration time depends mainly by the pressure step and the consequent magnitude of the compression or expansion effect of the gas in the measuring cell, and ranges in this work from (1 to 3.5) hours.

Gas measurements are started after equilibrium is reached. The sinkers and the compensation masses are alternatively weighed 15 times according to the following symmetrical sequence lasting 24 min:

S4 – S3 – cal – tare – S2 – S1 – S4 – S3 – S4 – S1 – S2 – tare – cal – S3 – S4.

Each object is suspended from, or placed on, the weighing line for 90 s and the data are recorded each second. To ensure stability of the measurements, only the last 30 s of collected data are used to calculate the system's outputs. Throughout the measurement sequence, temperature and pressure inside the measuring cell are also recorded each second.

3 Uncertainty Determination

According to the "Guide to the expression of uncertainty in measurement" (GUM) [22], once all of the uncertainty contributions have been determined, the combined standard uncertainty, u_c , can be calculated applying the law of uncertainty propagation (GUM JCGM 100:2008, chapter 5.1.2). This law is based on an n th-order Taylor series expansion and expresses u_c as squared sum of partial derivatives of the function multiplied by the uncertainty contributions.

Under the hypothesis that a first-order Taylor series is an acceptable approximation, the resulting equation for u_c is useful graphical representation of the uncertainty contributions and their sensitivity coefficients. Applying this hypothesis to the uncertainty determination of the density expressed by Eqs. 6–9 it is possible to obtain Eq. 13 for the calculation of the combined standard uncertainty of density measurements, $u_c(\rho)$:

$$\begin{aligned}
u_c(\rho) = & \left[\sum_{i=1}^6 \left(\frac{\partial \rho}{\partial m_i} \right)^2 \cdot u^2(m_i) + \sum_{i=1}^6 \left(\frac{\partial \rho}{\partial V_i} \right)^2 \cdot u^2(V_i) \right. \\
& + \sum_{i=1}^4 \left(\frac{\partial \rho}{\partial A_{S,i}} \right)^2 \cdot u^2(A_{S,i}) + \sum_{i=1}^6 \left(\frac{\partial \rho}{\partial W_i} \right)^2 \cdot u^2(W_i) \\
& + \left(\frac{\partial \rho}{\partial \rho_{\text{air}}} \right)^2 \cdot u^2(\rho_{\text{air}}) + \left(\frac{\partial \rho}{\partial \rho_{\text{cond}}} \right)^2 \cdot u^2(\rho_{\text{cond}}) \\
& \left. + \left(\frac{\partial \rho}{\partial p} \right)^2 \cdot u^2(p) + \left(\frac{\partial \rho}{\partial T} \right)^2 \cdot u^2(T) \right]^{\frac{1}{2}}.
\end{aligned} \tag{13}$$

The partial derivatives in Eq. 13 are expressed as general terms and for clarity the uncertainty contributions are collected according thematic sources of uncertainty (e.g., mass, volume, etc.). The index i from 1 to 4 indicates the four sinkers, and from 5 to 6 the two compensation masses. The uncertainty terms will be described later in Sect. 3.1.

However, such a clear description is not fully representative of the system of equations described in this work, which is characterized by a significant nonlinearity. Hence, the first-order expansion might not be an acceptable approximation and higher-order Taylor series expansion terms should be added to Eq. 13 (GUM JCGM 100:2008, chapter 5.1.2 NOTE). Furthermore, calculation of the partial derivatives for this system is very challenging.

For these reasons, a more accessible methodology for the estimation of the uncertainty was developed. Under the assumption that all input quantities are independent, the uncertainties of the six outputs (α , β , ϕ , γ_3 , γ_4 , and ρ_{fluid}) were determined through the following two steps: (1) determination of all uncertainty contributions according to GUM (JCGM 100:2008, chapter 4), and (2) application of the sensitivity analysis method to obtain the combined standard uncertainty.

This methodology differs from the GUM method only in the second part, providing a practical approach to evaluating experimental uncertainty, and bypassing the complexity of partial derivations. The sensitivity analysis method is a numerical approximation of the GUM that consists of running as many mathematical iterations of the working equations as the number of uncertainty contributions. For each iteration, one uncertainty contribution is added to the respective measured, estimated, or assumed value. A new, distorted value of the output under consideration is obtained, and its squared difference from the original value is calculated. The combined standard uncertainty, u_c , is estimated with the square root of the sum of all these squared differences according to Eq. 14:

$$u_c(\bar{X}) = \left[\sum_{i=1}^N (X_i - \bar{X})^2 \right]^{\frac{1}{2}}, \tag{14}$$

where \bar{X} is the original system's output for which an uncertainty estimation is required, N is the number of uncertainty contributions estimated using the first step

of this methodology, and X_i is the distorted value of the output after applying the uncertainty contribution i .

The sensitivity analysis method was validated with systems of various degrees of complexity and compared to the method described by GUM. Despite showing a slight over estimation of the uncertainty, it provides comparable results to the GUM. Furthermore, it has been shown to be reliable, easy to use, and fast. A more detailed description of this method, including its validation and application, will be presented in a companion paper to be submitted following this work [23].

3.1 Uncertainty Contributions

3.1.1 Mass

The standard uncertainty in the mass of the weighed object, $u(m)$, is already a combined uncertainty determined through the analysis of the mass calibration method. This calibration consists of a double substitution method with the use of reference and sensitivity masses. The uncertainty, reported in Table 1, ranges between (9 and 14) μg depending on the object.

3.1.2 Volume

The standard uncertainty in the volume of the weighed object, $u(V)$, is obtained from the analysis of the calibration method. The volume of each object was calibrated by means of a hydrostatic comparator using reference silicon standards and sensitivity masses. The uncertainty, reported in Table 1, ranges between (0.1 and 0.3) mm^3 depending of the object.

3.1.3 Surface

The standard uncertainty in the surface of the sinkers, $u(A_S)$, has two contributions. The relative uncertainty of the geometrical surface considering manufacturing tolerances was estimated to be 0.45% of the surface itself. And the relative uncertainty in the estimation of the surface enlargement factor was estimated to be 0.03% of the surface. Since the second contribution is negligible compared to the first, 0.45% was assumed as the relative standard uncertainty in the surface of the sinkers.

3.1.4 Weighing

The standard uncertainty in the weighing, $u(W)$, is a combination of individual uncertainties of the analytical balance (reproducibility, span and linearity), and the

average standard deviation of measurements. For the weighing range of the four sinker densimeter, (32 to 62) g, the standard uncertainty was estimated to be 20 μg .

3.1.5 Air Density

The density of the air can be determined quite accurately using an empirical equation. Major contributions to the uncertainty of ρ_{air} are the standard deviation of the measurements over the investigated period and the uncertainty in the measurements of T_{air} , p_{air} , φ_{air} . The standard uncertainty in the air density, $u(\rho_{\text{air}})$, was estimated to be equal to 0.01 $\text{kg} \cdot \text{m}^{-3}$.

3.1.6 Condensate Density

For gases for which ρ_{cond} is assumed to be a constant value, its tentative uncertainty is provided in literature [8, 9]. In this case, the relative standard uncertainty in the density of the condensate, $u(\rho_{\text{cond}})/\rho_{\text{cond}}$, is hypothesized to be 10%, however, this value might be much bigger.

When ρ_{cond} is determined using molecular dynamics simulation (MDS), its uncertainty can be divided into two contributions. One is the uncertainty of the calculation of ρ_{dew} using the equation of state (e.g., $u(\rho_{\text{dew}})/\rho_{\text{dew}} = 0.03\%$ for CO_2 calculated with the EOS of Span and Wagner [24]). The other is the relative standard deviation of MDS, estimated to be 10% of ρ_{cond} . Since the first contribution is usually negligible compared to the second, $u(\rho_{\text{cond}})/\rho_{\text{cond}}$ is estimated to be 10%.

3.1.7 Pressure

The standard uncertainty in the pressure measurement, $u(p)$, is equal to 0.45 kPa and includes the uncertainty in the calibration using the piston gauge and the standard deviation of the measurements.

3.1.8 Temperature

The standard uncertainty in the temperature measurement, $u(T)$, is a combination of individual uncertainties of the calibration procedures (triple point of water and freezing point of indium), the temperature measuring chain (resistance bridge and reference resistor), and the measurement itself (gradient across the measuring cell and standard deviation). In the range between (0 to 430) K the estimated combined standard uncertainty in the measured temperature is 6.2 mK.

3.2 Combined Uncertainty in Density and Adsorption

Using the sensitivity analysis method it was possible to estimate the combined standard uncertainty in density, $u_c(\rho_{\text{fluid}})$, and adsorption, $u_c(\gamma)$. To report

Table 2 Comparison of the FSD uncertainty in density and adsorption measurements with the previous state of the art. (The given literature references provide detailed information on the respective uncertainties.)

	FSD [this work]	2SD [1, 10, 20]	TSD [8, 9]
Density range [$\text{kg} \cdot \text{m}^{-3}$]	5.7 to 180 (tested)	1 to 2000	13.7 to 137.2
$U_c(\rho) (k = 2)$ [$\text{kg} \cdot \text{m}^{-3}$]	0.0034 to 0.0190	0.0012 to 0.10	0.020
Adsorption range [$\mu\text{g} \cdot \text{cm}^{-2}$]	0.10 to 2.32 (tested)	–	0.05 to 3.95
$U_c(\gamma) (k = 2)$ [$\mu\text{g} \cdot \text{cm}^{-2}$]	0.16 to 0.26	–	1.02 to 1.51

these uncertainties, a level of confidence equal to 95% described by the coverage factor $k = 2$ (GUM JCGM 100:2008, chapter 6) was chosen. For the investigations conducted in this work, the resulting combined expanded uncertainties were $U_c(\rho_{\text{fluid}}) = (0.0034 \text{ to } 0.019) \text{ kg} \cdot \text{m}^{-3}$ for density measurements and $U_c(\gamma) = (0.16 \text{ to } 0.26) \mu\text{g} \cdot \text{cm}^{-2}$ for adsorption measurements.

In Table 2 the uncertainties of the FSD are compared to the previous state of the art, namely the 2SD for density measurements [1, 20], and the TSD for adsorption measurements [8, 9]. The estimated uncertainty of the FSD in the investigated range of density is comparable to that of the 2SD. The major achievement of the FSD in terms of uncertainties is in the adsorption measurements. For the investigated range, the estimated uncertainty in adsorption is one order of magnitude smaller compared to the TSD.

4 First Experimental Results

4.1 Experimental Materials

Details of the gasses used are included in Table 3. Mixtures were prepared at the Bundesanstalt für Materialforschung und -prüfung (BAM, Berlin, Germany) using a gravimetric technique.

4.2 Pure Gases Density

Density measurements were conducted on argon (Ar) and nitrogen (N_2) to validate the instrument. Both fluids have well established equations of state (EOS) and have been widely reported in literature. Furthermore, they are cheap, can be purchased at high purity, and are safe to handle. For these reasons, they are perfect candidates to be used as reference standards for the validation of gravimetric instruments.

Table 3 Description of gas samples investigated

Chemical name	CAS number	Supplier	Purity / mole fraction
Argon	7440-37-1	Air Liquide	0.999999 ^a
Nitrogen	7727-37-9	Air Liquide	0.999999 ^b
Carbon dioxide	124-38-9	Air Liquide	0.999995 ^c
Propane	74-98-6	Matheson	0.99999 ^d
(0.75 CO ₂ + 0.25 C ₃ H ₈)	-	BAM	0.74981/0.25019 ^e

^aAmount of impurities as stated by the supplier: H₂O < 0.5 mol ppm, O₂ < 0.1 mol ppm, CO < 0.1 mol ppm, CO₂ < 0.1 mol ppm, CnHm < 0.1 mol ppm, H₂ < 0.1 mol ppm

^bAmount of impurities as stated by the supplier: H₂O < 0.5 mol ppm, O₂ < 0.1 mol ppm, CnHm < 0.1 mol ppm, CO < 0.1 mol ppm, CO₂ < 0.1 mol ppm, H₂ < 0.1 mol ppm, HHCs < 1 mol ppb

^cAmount of impurities as stated by the supplier: H₂O < 2 ppmv, O₂ < 1 ppmv, HHCs < 0.1 ppmv, N₂ < 2 ppmv, CO < 0.5 ppmv, NO_x < 0.1 ppmv

^dAmount of impurities as stated by the supplier: C₂O < 1 mol ppm, N₂ < 2 mol ppm, O₂ < 1 mol ppm, CnHm < 8 mol ppm, C₃H₆ < 2 mol ppm, H₂O < 2 mol ppm

^eAmount of impurities as stated by the supplier: N₂ < 0.0001 mol%, C₃H₆ < 0.000025 mol%, O₂ < 0.000025 mol%, CO < 0.000022 mol%, NO < 0.000004 mol%

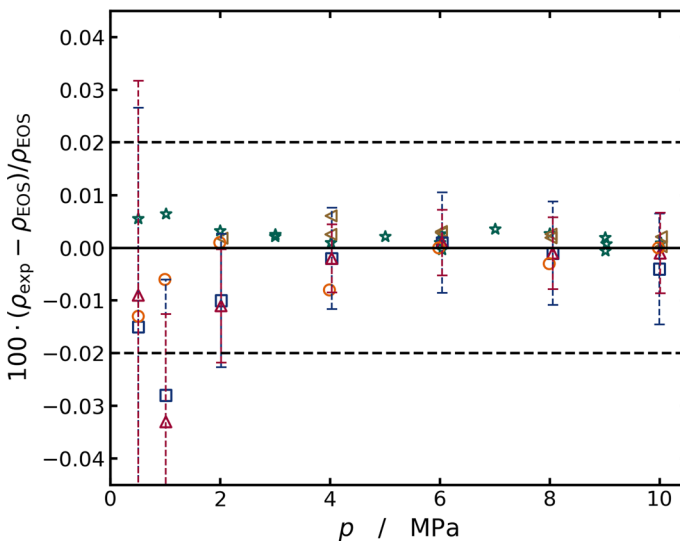


Fig. 5 Relative deviation of the experimental density of argon, ρ_{exp} , from the density calculated with the equation of state of Tegeler *et al.* [25], ρ_{EOS} . The relative deviation in % is plotted versus pressure. Measurements conducted in this work are reported with error bars indicating the relative combined expanded uncertainty ($k = 2$). The dashed lines indicate the uncertainty interval of the EOS ($\pm 0.02\%$). \square – This work, $T = 283$ K; \triangle – This work, $T = 293$ K; \circ – This work, $T = 293$ K conducted using a piston gauge as a main pressure sensor; \star – Reference measurements at $T = 280$ K, Gilgen *et al.* [26]; \triangleleft – Reference measurements at $T = 280$ K, Klimeck *et al.* [27]

Two isotherms were investigated, (283 and 293) K, up to the pressure of 10 MPa for both Ar and N₂. The measured range in density was (5.7 to 180) kg · m⁻³. The combined expanded uncertainty ($k = 2$) in density measurements ranged between

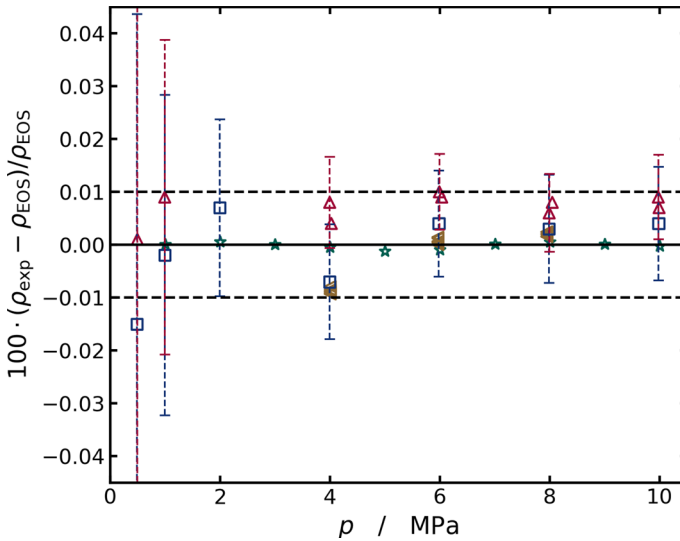


Fig. 6 Relative deviation of the experimental density of nitrogen, ρ_{exp} , from the density calculated with the equation of state of Span *et al.* [28], ρ_{EOS} . The relative deviation in % is plotted versus pressure. Measurements conducted in this work are reported with error bars indicating the relative combined expanded uncertainty ($k = 2$). The dashed lines indicate the uncertainty interval of the EOS ($\pm 0.01\%$). \square – This work, $T = 283$ K; \triangle – This work, $T = 293$ K; \star – Reference measurements at $T = 293$ K, Nowak *et al.* [29]; \triangleleft – Reference measurements at $T = 293$ K, McLinden and Loesch [1]

(0.0034 to 0.0190) $\text{kg} \cdot \text{m}^{-3}$, corresponding to (0.060 to 0.011)%. The density isotherms are provided in the supplementary information as machine readable files.

In Fig. 5 the relative deviation of Ar densities from the EOS of Tegeler *et al.* [25] is plotted versus pressure for the two isotherms investigated. The uncertainty of the equation is reported by the authors to be 0.02%. The FSD data include error bars indicating the relative combined expanded uncertainty ($k = 2$). To provide a comprehensive validation of the FSD, the measurement at 293 K was repeated using a piston gauge as a reference pressure sensor. The use of the piston gauge requires modifications of the measuring setup and extends the time necessary to complete the measurement procedure, but provides a higher level of accuracy in pressure measurements. In addition to the experimental data the literature data from Gilgen *et al.* [26] and Klimeck *et al.* [27] are shown in Fig. 5 for comparison. Those two data sets, which were also obtained using gravimetric instruments, were used by Tegeler to fit the EOS.

Overall, the density of Ar measured with the FSD is in very good agreement with the EOS and the literature data. The maximum deviation from the EOS is 0.004% for $p > 2$ MPa; it increases at lower pressures (max. 0.033%) due to the increased measurement uncertainty. On the other hand, the data measured using the piston gauge agree with the EOS within 0.013% for the whole pressure range investigated.

In Fig. 6 the relative deviation of N_2 densities from the EOS of Span *et al.* [28] is plotted versus pressure for the two isotherms investigated. The uncertainty of

the equation is reported by the authors to be 0.01%. The FSD data include error bars indicating the relative combined expanded uncertainty ($k = 2$). Literature data (Nowak et al. [29] and McLinden and Lösch [1]) are also shown for comparison.

The density of N_2 measured with the FSD is within the uncertainty interval of the EOS for the whole pressure range investigated. The maximum deviation is 0.015% obtained at the lowest pressure measured (0.5 MPa), for which the highest uncertainty is estimated. Furthermore, repeatability measurements show the consistency of the FSD investigation obtaining an average difference in relative deviation of 0.0023% for densities measured at the same pressure points (see data at 4, 6, 8, and 10 MPa).

4.3 Pure Gases Adsorption

Adsorption on the gold surfaces of sinkers 1, 2, and 3 were determined for carbon dioxide (CO_2) and propane (C_3H_8) to validate the instrument for adsorption measurements. A gold surface is a quasi nonporous material on which a very small amount of gas adsorbs, especially in conditions far away from the dew line. For this reason, this type of investigation requires high resolution. In the literature, only the adsorption of carbon monoxide (CO) on gold (Au) using non gravimetric techniques is broadly reported, in an effort to characterize gold as active catalyst for CO oxidation at low temperature [30]. CO_2 adsorption on gold surfaces has been reported only by Yang and Richter using a tandem-sinker densimeter investigating CO_2 and C_2H_6 adsorption on stainless steel and gold surfaces [31].

Two isotherms were investigated using the FSD: 283 K up to the saturation pressure of about 4.5 MPa for CO_2 , and 293 K up to the saturation pressure of about 0.84 MPa for C_3H_8 . The measured range in adsorption load was (0.18 to 2.32) $\mu g \cdot cm^{-2}$ for CO_2 and (0.10 to 1.50) $\mu g \cdot cm^{-2}$ for C_3H_8 . The combined expanded uncertainty ($k = 2$) in adsorption measurements ranged between (0.16 to 0.26) $\mu g \cdot cm^{-2}$ for CO_2 and (0.16 to 0.18) $\mu g \cdot cm^{-2}$ for C_3H_8 . The adsorption isotherms are provided in the supplementary information as machine readable files according to the Adsorption Information Format (AIF) [32], a universal adsorption format. To provide an additional source of comparison, the same adsorption isotherms were also investigated using a TSD available at Chemnitz University of Technology (TUC). This is a well-established apparatus developed for the investigation of adsorption on porous and quasi nonporous materials, however, for very low adsorption loads the relative measuring uncertainty is quite high.

In Fig. 7 the adsorption load, γ , for CO_2 at 283 K is plotted versus pressure. Adsorption measured with the FSD is compared to two datasets measured with a TSD, one measured as part of this work (at TUC) and one reported by Yang and Richter [31]. Error bars indicating the combined expanded uncertainty ($k = 2$) are reported for all FSD data points and for a couple of points in the comparison measurements (TSD).

The improvement in the measuring technology of the FSD is clearly visible in Fig. 7. Specifically, the measuring uncertainty of the FSD is one order of magnitude lower compared to the TSD (previous state of the art). Furthermore, thanks to

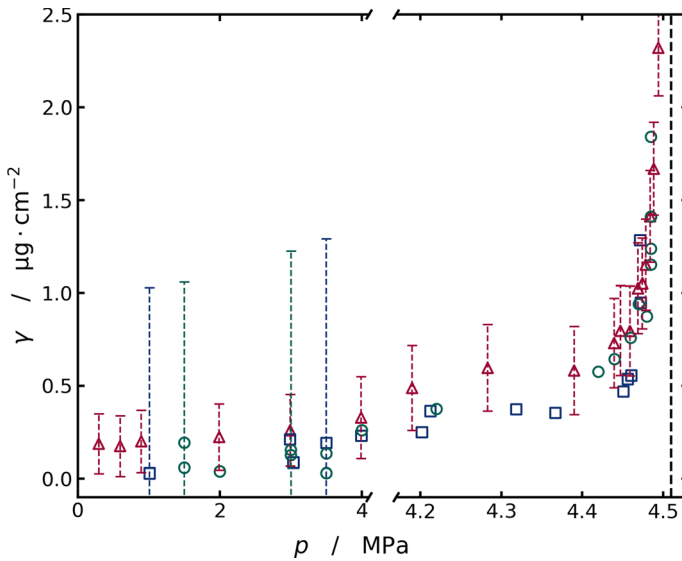


Fig. 7 Adsorption of carbon dioxide on the gold surfaces of sinkers 1, 2, and 3. The adsorption load, γ , in $\mu\text{g} \cdot \text{cm}^{-2}$, is plotted versus pressure up to the saturation pressure of CO_2 at $T = 283 \text{ K}$, $p_{\text{sat}} \approx 4.5 \text{ MPa}$ (dashed line). Measurements conducted in this work are reported with error bars indicating the combined expanded uncertainty ($k = 2$). For comparison, two error bars are also plotted for the TSD measurements. \triangle – This work, $T = 283 \text{ K}$; \square – Measurements conducted using a TSD (at TUC) at $T = 283 \text{ K}$; \circ – Reference measurements at $T = 283 \text{ K}$, Yang and Richter [31]

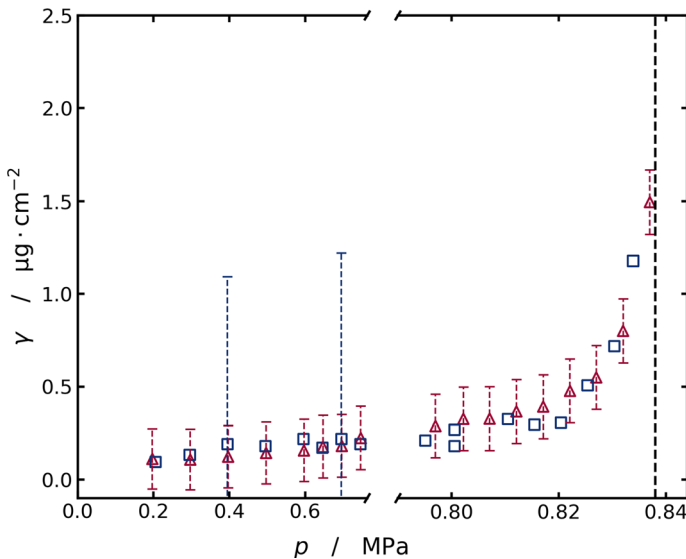


Fig. 8 Adsorption of propane on the gold surfaces of sinkers 1, 2, and 3. The adsorption load, γ , in $\mu\text{g} \cdot \text{cm}^{-2}$, is plotted versus pressure up to the saturation pressure of C_3H_8 at $T = 293 \text{ K}$, $p_{\text{sat}} \approx 0.84 \text{ MPa}$ (dashed line). Measurements conducted in this work are reported with error bars indicating the combined expanded uncertainty ($k = 2$). For comparison two error bars are plotted also for the TSD measurements. \triangle – This work, $T = 293 \text{ K}$; \square – Measurements conducted using a TSD (at TUC) at $T = 293 \text{ K}$

the increased resolution of adsorption measurement, the FSD adsorption isotherm shows a smoother trend, especially approaching the dew line, and positive values at very low pressures; with the TSD, negative adsorption values at low pressure can be calculated, which are physically not possible, of course.

In Fig. 8 the adsorption load, γ , for C_3H_8 at $T = 293$ K is plotted versus pressure. Adsorption measured with the FSD is compared to the dataset measured with the TSD as part of this work (at TUC). Error bars indicating the combined expanded uncertainty ($k = 2$) are reported for all FSD data points and for a couple of points in the comparison measurement.

The two datasets reported in Fig. 8 show good agreement, and, as was the case for CO_2 , data obtained with the FSD have a much lower uncertainty compared to the TSD data and follow a smoother trend while approaching the saturation pressure.

4.4 Density and Adsorption of a Gas Mixture

After validating the FSD with pure gases density and adsorption measurements, the apparatus was used to investigate a ($0.75 CO_2 + 0.25 C_3H_8$) binary mixture. The mixture was prepared using a gravimetric method at the Bundesanstalt für Materialforschung und -prüfung (BAM, Berlin, Germany). Details on the actual composition of the mixture can be found in Table 3. One isotherm was investigated at a temperature of 283 K and pressures up to the saturated vapor-pressure of the mixture ($p_{sat} \approx 2.47$ MPa). Both density and adsorption results are reported in the supplementary information as machine readable files.

4.4.1 Density

Density was investigated in the range between (9.6 and 59.6) $kg \cdot m^{-3}$ with combined expanded uncertainties ($k = 2$) in the range of (0.0038 to 0.0058) $kg \cdot m^{-3}$. Results were compared to the GERG-2008 model of Kunz and Wagner [33], a wide-range EOS for natural gases and other mixtures. For the binary mixture, and for the T, p ranges investigated in this work, the uncertainty of the equation is reported by the authors to be 0.3%.

In Fig. 9 the relative deviation of the experimental density compared to the EOS is plotted versus pressure. This deviation, which increases when approaching the saturation pressure, is well inside the uncertainty interval of the EOS. The error bars in Fig. 9 represent the relative combined expanded uncertainty ($k = 2$) in density measurements. However, this uncertainty does not include the uncertainty in composition of the gas mixture and uncertainty related to the shift of the composition due to selective adsorption. The mixture EOS approaches the ideal-gas limit at zero pressure, and a systematic deviation of the experimental data from this limit could indicate an incorrect composition. However, for the investigated ($0.75 CO_2 + 0.25 C_3H_8$) mixture such composition uncertainties have a small impact on the determination of the density at low pressures since the two components have almost the same molar mass (44.0094 $g \cdot mol^{-1}$ for CO_2 , and 44.0958 $g \cdot mol^{-1}$ for C_3H_8) [34]. For these reasons, to further evaluate the results, the density measurements were

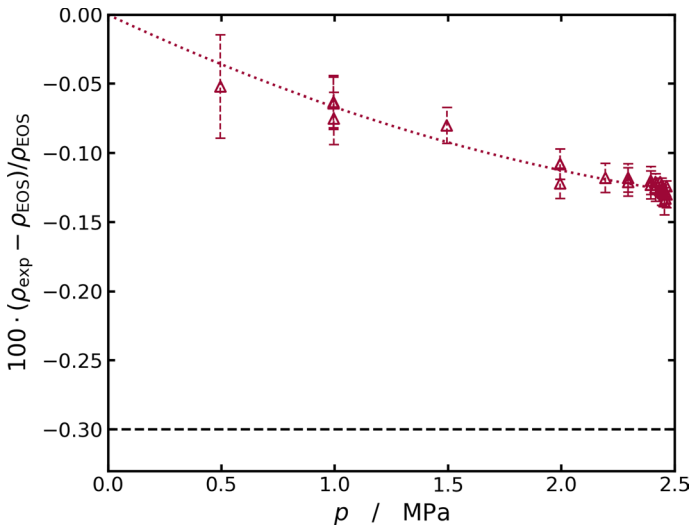


Fig. 9 Relative deviation of the experimental density of a (0.75 CO₂ + 0.25 C₃H₈) mixture, ρ_{exp} , from the density calculated with the equation of state GERG-2008 Kunz and Wagner [33], ρ_{EOS} . The relative deviation in % is plotted versus pressure. Measurements are reported with error bars indicating the relative combined expanded uncertainty ($k = 2$). The dashed line indicates the uncertainty interval of the EOS ($\pm 0.3\%$). The dotted line represents the quadratic extrapolation of the experimental measurements to zero. \triangle – This work, $T = 283$ K

extrapolated to zero using a quadratic equation (see dotted line in Fig. 9). Even when the equation is forced to intersect the origin, all experimental data match, within the uncertainties, the quadratic extrapolation. In the range close to the dew line the data fall on the quadratic curve, and this additional validation proves the effectiveness of sorption effects correction on density measurements using the FSD.

Additionally, the measured densities were fitted to a virial expansion according to the following Eq. 15 [35]:

$$p = \frac{\rho RT}{M} \left[1 + B(T) \frac{\rho}{M} + C(T) \frac{\rho^2}{M^2} \right], \quad (15)$$

where p is the pressure, ρ is the mass density, R is the universal gas constant, and T is the temperature. $B(T)$ and $C(T)$ are the second and third virial coefficients and are fitted parameters. M is the molar mass and is used in Eq. 15 to express the virial coefficients in their conventional units on a molar basis. M can be computed independently by letting it be an additional fitted parameter, in this case it serves as consistency check on the gravimetric mixture composition.

The fitted virial coefficients, respectively $B(T) = -178.93 \text{ cm}^3 \cdot \text{mol}^{-1}$ and $C(T) = 7979.6 \text{ cm}^6 \cdot \text{mol}^{-2}$, are representative just for the investigated isotherm and mixture composition. The fitted molar mass, $M = 44.0128 \text{ g} \cdot \text{mol}^{-1}$, lies between the molar masses of the pure components (reported in the previous paragraph), and differs by 0.041% from the calculated molar mass of the mixture, $M_{\text{mix}} = 44.0310 \text{ g} \cdot \text{mol}^{-1}$. The relative deviations between the virial equation and

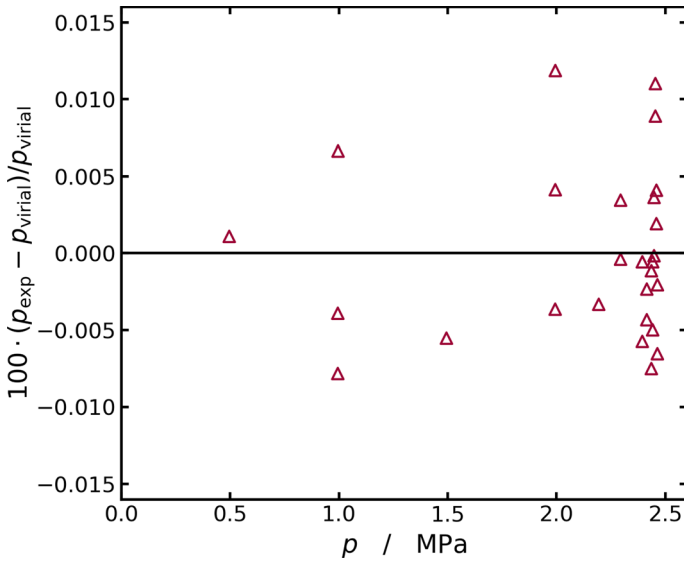


Fig. 10 Relative deviation of the experimental pressure, p_{exp} , from the pressure calculated with the virial Eq. 15, p_{virial} , for a (0.75 CO_2 + 0.25 C_3H_8) mixture. The relative deviation in % is plotted versus pressure. \triangle – This work, $T = 283$ K

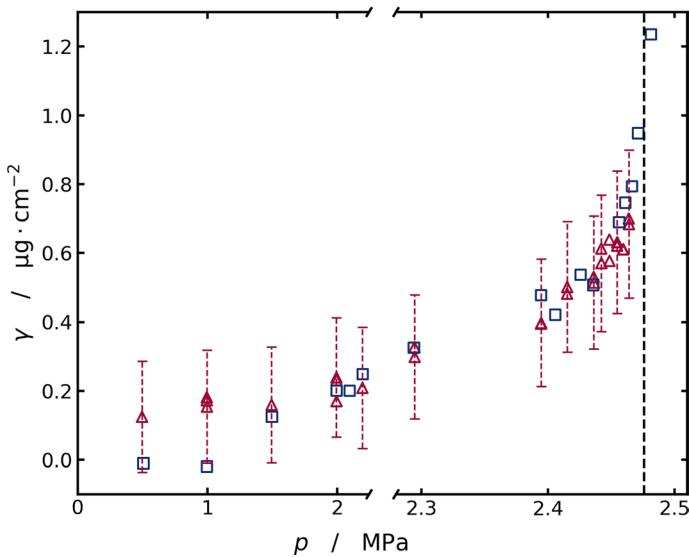


Fig. 11 Adsorption of a (0.75 CO_2 + 0.25 C_3H_8) mixture on the gold surfaces of sinkers 1, 2, and 3. The adsorption load, γ , in $\mu\text{g} \cdot \text{cm}^{-2}$, is plotted versus pressure up to the saturation pressure of the mixture at $T = 283$ K, $p_{\text{sat}} \approx 2.47$ MPa (dashed line). Measurements conducted in this work are reported with error bars indicating the combined expanded uncertainty ($k = 2$). \triangle – This work, $T = 283$ K; \square – Measurements conducted using a TSD (at TUC) at $T = 283$ K

the experimental measurements are shown in Fig. 10. All but two of the experimental points agree with the virial equation within 0.01%, including those close to the dew line. The data have no specific trend or offset, indicating the consistency of the FSD measurements and the effectiveness of sorption effects correction.

4.4.2 Adsorption

Adsorption loads of a (0.75 CO₂ + 0.25 C₃H₈) mixture on the sinkers' gold surface were investigated in the range between (0.12 and 0.70) μg · cm⁻². The combined expanded uncertainty ($k = 2$) ranges from (0.16 to 0.22) μg · cm⁻². In Fig. 11 the adsorption load, γ , at 283 K is plotted versus pressure. As was the case for pure CO₂ and C₃H₈, measurements conducted with the FSD are compared to the same isotherm measured with a TSD (at TUC). Error bars indicating the combined expanded uncertainty ($k = 2$) are reported for all FSD data points.

The two datasets plotted in Fig. 11 overall show good agreement except for the lower pressure range. In this range, the FSD provides better resolution compared to the TSD and avoids negative adsorption loads.

5 Conclusions

The Four-sinker Densimeter (FSD) was presented. This instrument was developed to increase the resolution in density and adsorption investigations for pure gases and gas mixtures. Furthermore, the FSD is able to correct sorption effects on density measurements, which is especially relevant close to the dew line. The apparatus covers a temperature range from (193 to 423) K and pressures up to 15 MPa. A thorough uncertainty analysis (explained in detail in a companion paper) was conducted. The combined expanded uncertainty ($k = 2$) was estimated to be between (0.0034 to 0.019) kg · m⁻³, corresponding to (0.060 to 0.011)% in density and (0.16 to 0.26) μg · cm⁻² in adsorption load for the ranges investigated.

The instrument was validated with density measurements on high-purity argon and nitrogen as well as adsorption investigations of carbon dioxide and propane on a gold surface. Density measurements for both Ar and N₂ at $T = (283 \text{ and } 293)$ K and pressures up to 10 MPa agree within uncertainty intervals with their respective equations of state and reference data. Adsorption loads of CO₂ at $T = 283$ K and C₃H₈ at $T = 293$ K on a gold surface, up to the dew-point pressure, agree overall with reference data and with data on the same isotherms measured using a tandem-sinker densimeter. Furthermore, adsorption isotherms measured with the FSD show a smoother trend and a better resolution at low pressures.

First experimental results for a (0.75 CO₂ + 0.25 C₃H₈) binary mixture were presented. Measurements were conducted along the 283 K isotherm and for pressures up to the mixture dew point. The density results were evaluated by extrapolation of a quadratic equation to zero density and the fitting of a virial equation. The agreement

of the experimental data with these equations proved the effectiveness of sorption effects correction on accurate density measurements.

The FSD alone is not able to correct for the selective adsorption of different components of a mixture. For this reason, the adsorption measurements conducted on pure gases and the binary gas mixture will be used to validate molecular dynamics simulation (MDS). With the help of MDS, which allows investigating the structure of the adsorbate on an atomistic scale, it will be possible to obtain density measurements corrected for the distorting adsorption effects. In the future, the apparatus will also be used to accurately determine dew-point densities and pressures of pure gases and gas mixtures.

Supplementary Information The online version contains supplementary material available at <https://doi.org/10.1007/s10765-024-03336-0>.

Acknowledgements For the precise work in fabricating some core densimeter parts, we are thankful to the team of Christian Gramann of the mechanical workshop at Ruhr-Universität Bochum (RUB). In this context, we are also thankful to Christian Hiltner and Michael Niesen of the institute's electronics development laboratory at RUB and to the electronics technician Hans-Joachim Knobloch of the applied thermodynamics group at Chemnitz University of Technology (TUC) for designing and fabricating customized measurement electronics. For the preparation of the specialty gas mixture studied in the present work, we thank Dr. Dirk Tuma from Bundesanstalt für Materialforschung (BAM). Moreover, for the precious IT support and assistance in the development of the highly sophisticated LabVIEW code we thank Dr. Gerrit Dresp. Finally, we want to thank Markus Sekulla from our group at Chemnitz University of Technology for the fruitful discussions and cooperation within the ongoing DFG project.

Author Contributions Conceptualization: RK, KM, MM and MR; Methodology: LB, RK, KM, MM and MR; Software: LB and KM; Validation: LB and MR; Formal Analysis: LB, MM and MR; Investigation: LB; Resources: RK, MM and MR; Data Curation: LB and KM; Writing - Original Draft: LB; Writing - Review & Editing: RK, MM and MR; Visualization: LB, KM and MR; Supervision: RK, MM and MR; Project Administration: MR; Funding Acquisition: MR.

Funding Open Access funding enabled and organized by Projekt DEAL. This work was funded by the Deutsche Forschungsgemeinschaft (DFG, German Research Foundation) – Project numbers 269357610 and 459051105.

Data Availability All data required to understand the present work are provided in the supplementary information.

Code Availability Not applicable.

Declarations

Conflict of interest The authors have no competing interests to declare that are relevant to the content of this paper.

Ethical Approval The work contains no libelous or unlawful statements, does not infringe on the rights of others, or contains material or instructions that might cause harm or injury.

Consent to Participate The authors consent to participate.

Consent for Publication All authors read the final version of the manuscript and consent to publish.

Open Access This article is licensed under a Creative Commons Attribution 4.0 International License, which permits use, sharing, adaptation, distribution and reproduction in any medium or format, as long as you give appropriate credit to the original author(s) and the source, provide a link to the Creative Commons licence, and indicate if changes were made. The images or other third party material in this article are included in the article's Creative Commons licence, unless indicated otherwise in a credit line to the material. If material is not included in the article's Creative Commons licence and your intended use is not permitted by statutory regulation or exceeds the permitted use, you will need to obtain permission directly from the copyright holder. To view a copy of this licence, visit <http://creativecommons.org/licenses/by/4.0/>.

References

1. M.O. McLinden, C. Lösch-Will, Apparatus for wide-ranging, high-accuracy fluid (p , ρ , T) measurements based on a compact two-sinker densimeter. *J. Chem. Thermodyn.* **39**, 507–530 (2007). <https://doi.org/10.1016/j.jct.2006.09.012>
2. W. Wagner, R. Kleinrahm, Densimeters for very accurate density measurements of fluids over large ranges of temperature, pressure, and density. *Metrologia* **41**, 24–39 (2004). <https://doi.org/10.1088/0026-1394/41/2/S03>
3. X. Yang, R. Kleinrahm, M.O. McLinden, M. Richter, The magnetic suspension balance: 40 years of advancing densimetry and sorption science. *Int. J. Thermophys.* **44**, 169 (2023). <https://doi.org/10.1007/s10765-023-03269-0>
4. M. Richter, R. Kleinrahm, Influence of adsorption and desorption on accurate density measurements of gas mixtures. *J. Chem. Thermodyn.* **74**, 58–66 (2014). <https://doi.org/10.1016/j.jct.2014.03.020>
5. M. Richter, M. McLinden, Densimetry for the quantification of sorption phenomena on nonporous media near the dew point of fluid mixtures. *Sci. Rep.* **7**, 6185 (2017). <https://doi.org/10.1038/s41598-017-06228-6>
6. K. Brachthäuser, R. Kleinrahm, H.W. Lösch, W. Wagner, Entwicklung eines neuen dichtemeßverfahrens und aufbau einer hochtemperatur-hochdruck-dichtemeßanlage. *Fortschr.-Ber. VDI vol. 371* (1993)
7. M. Richter, R. Kleinrahm, R. Lentner, R. Span, Development of a special single-sinker densimeter for cryogenic liquid mixtures and first results for a liquefied natural gas (LNG). *J. Chem. Thermodyn.* **93**, 205–221 (2016). <https://doi.org/10.1016/j.jct.2015.09.034>
8. R. Kleinrahm, X. Yang, M.O. McLinden, M. Richter, Analysis of the systematic force-transmission error of the magnetic-suspension coupling in single-sinker densimeters and commercial gravimetric sorption analyzers. *Adsorption* **25**, 717–735 (2019). <https://doi.org/10.1007/s10450-019-00071-z>
9. X. Yang, R. Kleinrahm, M.O. McLinden, M. Richter, Uncertainty analysis of adsorption measurements using commercial gravimetric sorption analyzers with simultaneous density measurement based on a magnetic-suspension balance. *Adsorption* **26**, 645–659 (2020). <https://doi.org/10.1007/s10450-020-00236-1>
10. R. Kleinrahm, W. Wagner, Measurement and correlation of the equilibrium liquid and vapour densities and the vapour pressure along the coexistence curve of methane. *J. Chem. Thermodyn.* **18**, 739–760 (1986). [https://doi.org/10.1016/0021-9614\(86\)90108-4](https://doi.org/10.1016/0021-9614(86)90108-4)
11. M. McLinden, M. Richter, Application of a two-sinker densimeter for phase-equilibrium measurements: A new technique for the detection of dew points and measurements on the (methane + propane) system. *J. Chem. Thermodyn.* **99**, 105–115 (2016). <https://doi.org/10.1016/j.jct.2016.03.035>
12. K. Moritz, R. Kleinrahm, M.O. McLinden, M. Richter, Development of a new densimeter for the combined investigation of dew-point densities and sorption phenomena of fluid mixtures. *Meas. Sci. Technol.* **28**, 127004 (2017). <https://doi.org/10.1088/1361-6501/aa940a>
13. K. Moritz, Dew-point densities of fluid mixtures. Doctoralthesis, Ruhr-Universität Bochum, Universitätsbibliothek (2020). <https://doi.org/10.13154/294-7626>

14. F. Reischbach, H.W. Lösch, Magnetic suspension balance for simultaneous measurement of a sample and the density of the measuring fluid. *J. Therm. Anal. Calorim.* **62**, 515–521 (2000). <https://doi.org/10.1023/a:1010179306714>
15. M.O. McLinden, R. Kleinrahm, W. Wagner, Force transmission errors in magnetic suspension densimeters. *Int. J. Thermophys.* **28**, 429–448 (2007). <https://doi.org/10.1007/s10765-007-0176-0>
16. S. Cavenati, C.A. Grande, A.E. Rodrigues, Adsorption equilibrium of methane, carbon dioxide, and nitrogen on zeolite 13X at high pressures. *J. Chem. Eng. Data* **49**, 1095–1101 (2004). <https://doi.org/10.1021/je0498917>
17. E.W. Lemmon, I.H. Bell, M.L. Huber, M.O. McLinden, NIST Standard Reference Database 23: Reference Fluid Thermodynamic and Transport Properties-REFPROP, Version 10.0, National Institute of Standards and Technology (2018). <https://doi.org/10.18434/T4/1502528>
18. M. Sekulla, M. Kohns, M. Richter, Adsorption of CO₂ on gold surfaces: adsorbate density assumption investigated using molecular dynamics simulations. *Ind. Eng. Chem. Res.* (2023). <https://doi.org/10.1021/acs.iecr.3c01993>
19. G.L. Harris, J.A. Torres, Selected laboratory and measurement practices and procedures to support basic mass calibrations. NISTIR (2003). <https://doi.org/10.6028/NIST.IR.6969-2018>
20. M.O. McLinden, J.D. Splett, A liquid density standard over wide ranges of temperature and pressure based on toluene. *J. Res. Natl. Inst. Stand. Technol.* **113**, 29–67 (2008). <https://doi.org/10.6028/jres.113.005>
21. H. Preston-Thomas, The international temperature scale of 1990(ITS-90). *Metrologia* **27**, 3–10 (1990). <https://doi.org/10.1088/0026-1394/27/1/002>
22. J.C.G.M. Jcgm, Evaluation of measurement data-guide to the expression of uncertainty in measurement. *Int. Organ. Stand. Geneva* **50**, 134 (2008)
23. L. Bernardini, M.O. McLinden, X. Yang, M. Richter, How accurate are your experimental data? - A more accessible methodology for uncertainty evaluation based on the GUM. *Int. J. Thermophys.* (2024 - to be submitted)
24. R. Span, W. Wagner, A new equation of state for carbon dioxide covering the fluid region from the triple-point temperature to 1100 K at pressures up to 800 MPa. *J. Phys. Chem. Ref. Data* **25**, 1509–1596 (1996). <https://doi.org/10.1063/1.555991>
25. C. Tegeler, R. Span, W. Wagner, A new equation of state for argon covering the fluid region for temperatures from the melting line to 700 K at pressures up to 1000 MPa. *J. Phys. Chem. Ref. Data* **28**, 779–850 (1999). <https://doi.org/10.1063/1.556037>
26. R. Gilgen, R. Kleinrahm, W. Wagner, Measurement and correlation of the (pressure, density, temperature) relation of argon I. The homogeneous gas and liquid regions in the temperature range from 90 K to 340 K at pressures up to 12 MPa. *J. Chem. Thermodyn.* **26**, 383–398 (1994). <https://doi.org/10.1006/jcht.1994.1048>
27. J. Klimeck, R. Kleinrahm, W. Wagner, An accurate single-sinker densimeter and measurements of the (p , ρ , T) relation of argon and nitrogen in the temperature range from (235 to 520) K at pressures up to 30 MPa. *J. Chem. Thermodyn.* **30**, 1558–1571 (1998). <https://doi.org/10.1006/jcht.1998.0421>
28. R. Span, E.W. Lemmon, T., J.R., W. Wagner, A. Yokozeki, A reference equation of state for the thermodynamic properties of nitrogen for temperatures from 63.151 to 1000 K and pressures to 2200 MPa. *J. Phys. Chem. Ref. Data* **29**, 1361–1433 (2000) <https://doi.org/10.1063/1.1349047>
29. P. Nowak, R. Kleinrahm, W. Wagner, Measurement and correlation of the (p , ρ , T) relation of nitrogen. I. The homogeneous gas and liquid regions in the temperature range from 66 K to 340 K at pressures up to 12 MPa. *J. Chem. Thermodyn.* **29**, 1137–1156 (1997). <https://doi.org/10.1006/jcht.1997.0230>
30. W.L. Yim, T. Nowitzki, M. Necke, H. Schnars, P. Nickut, J. Biener, M.M. Biener, V. Zielasek, K. Al-Shamery, T. Klüner, M. Bäumer, Universal phenomena of CO adsorption on gold surfaces with low-coordinated sites. *J. Phys. Chem. C* **111**, 445–451 (2007). <https://doi.org/10.1021/jp0665729>
31. X. Yang, M. Richter, Experimental investigation of surface phenomena on quasi nonporous and porous materials near dew points of pure fluids and their mixtures. *Ind. Eng. Chem. Res.* **59**, 3238–3251 (2020). <https://doi.org/10.1021/acs.iecr.9b06753>
32. J.D. Evans, V. Bon, I. Senkovska, S. Kaskel, A universal standard archive file for adsorption data. *Langmuir* **37**, 4222–4226 (2021). <https://doi.org/10.1021/acs.langmuir.1c00122>

33. O. Kunz, W. Wagner, The GERG-2008 wide-range equation of state for natural gases and other mixtures: an expansion of GERG-2004. *J. Chem. Eng. Data* **57**, 3032–3091 (2012). <https://doi.org/10.1021/je300655b>
34. T. Prohaska, J. Irrgeher, J. Benefield, J.K. Böhlke, L.A. Chesson, T.B. Coplen, T. Ding, P.J.H. Dunn, M. Gröning, N.E. Holden, H.A.J. Meijer, H. Moossen, A. Possolo, Y. Takahashi, J. Vogl, T. Walczyk, J. Wang, M.E. Wieser, S. Yoneda, X.-K. Zhu, J. Meija, Standard atomic weights of the elements 2021 (IUPAC Technical Report). *Pure Appl. Chem.* **94**(5), 573–600 (2022). <https://doi.org/10.1515/pac-2019-0603>
35. M. Richter, M.O. McLinden, Vapor-phase (p , ρ , T , x) behavior and virial coefficients for the (methane + propane) system. *J. Chem. Eng. Data* **59**, 4151–4164 (2014). <https://doi.org/10.1021/je500792x>

Publisher's Note Springer Nature remains neutral with regard to jurisdictional claims in published maps and institutional affiliations.

Authors and Affiliations

Luca Bernardini¹  · Reiner Kleinrahm² · Katharina Moritz¹  ·
Mark O. McLinden³  · Markus Richter¹ 

✉ Markus Richter
m.richter@mb.tu-chemnitz.de

¹ Applied Thermodynamics, Chemnitz University of Technology, Chemnitz 09107, Germany

² Thermodynamik, Ruhr University Bochum, Bochum 44780, Germany

³ Applied Chemicals and Materials Division, National Institute of Standards and Technology, Boulder, CO 80305, USA